Discovery and structural characterization of a thermostable bacterial monoamine oxidase

Lars L. Santema[1], Lorenzo Basile[2], Claudia Binda[2] and Marco W. Fraaije[1]

1 Molecular Enzymology, University of Groningen, The Netherlands
2 Department of Biology and Biotechnology, University of Pavia, Italy

Monoamine oxidases (MAOs) are pivotal regulators of neurotransmitters in mammals, while microbial MAOs have been shown to be valuable biocatalysts for enantioselective synthesis of pharmaceutical compounds or precursors thereof. To extend the knowledge of how MAOs function at the molecular level and in order to provide more biocatalytic tools, we set out to identify and study a robust bacterial variant: a MAO from the thermophile *Thermoanaerobacterales* bacterium (MAO_{Tb}). MAO_{Tb} is highly thermostable with melting temperatures above 73 °C and is well expressed in *Escherichia coli*. Substrate screening revealed that the oxidase is most efficient with *n*-alkylamines with *n*-heptylamine being the best substrate. Presteady-state kinetic analysis shows that reduced MAO_{Tb} rapidly reacts with molecular oxygen, confirming that it is a *bona fide* oxidase. The crystal structure of MAO_{Tb} was resolved at 1.5 Å and showed an exceptionally high similarity with the two human MAOs, MAO A and MAO B. The active site of MAO_{Tb} resembles mostly the architecture of human MAO A, including the cysteinyl protein–FAD linkage. Yet, the bacterial MAO lacks a C-terminal extension found in human MAOs, which explains why it is expressed and purified as a soluble protein, while the mammalian counterparts are anchored to the membrane through an α-helix. MAO_{Tb} also displays a slightly different active site access tunnel, which may explain the specificity toward long aliphatic amines. Being an easy-to-express, thermostable enzyme, for which a high-resolution structure was elucidated, this bacterial MAO may develop into a valuable biocatalyst for synthetic chemistry or biosensing.

Introduction

Biogenic amines are organic bases with one or more nitrogen groups. They are often formed by the decarboxylation of amino acids [1]. Their biological roles are numerous and they play important roles in various processes such as antioxidants and as neurotransmitters [2,3]. Besides their biological relevance, their detection is of economic importance as they are widely used as a marker for the quality of food. Also, high levels of biogenic amines are toxic for human consumption [4,5]. The detection of biogenic amines, especially in food, is often done by chromatography methods [6]. These methods, while highly accurate, are often time-consuming and costly. Biosensors based on enzymes offer a rapid and economical competitive alternative for the detection of amines from microorganisms [7]. Amine oxidases are excellent tools for sensing of amines and can be used for the detection of minute amounts of amines. Apart from their use in

Abbreviations
CHAO, cyclohexylamine oxidase from *Brevibacterium oxydans*; MAO, monoamine oxidase; MAO_{Tb}, monoamine oxidase from *Thermoanaerobacterales* bacterium; PuO_{Rh}, putrescine oxidase from *Rhodococcus erythropolis*.

biosensors, amine oxidases are also attractive biocatalysts. It has been demonstrated that amine oxidases can be used for the generation of various high-value pharma compounds, allowing the synthesis of enantiopure amines [8].

Amine oxidases can be divided into two superfamilies, based on whether they utilize copper or flavin as a tightly bound redox cofactor [9]. The metal-free flavin-containing amine oxidases catalyze the oxidation of primary and secondary amines by utilizing molecular oxygen as electron acceptor, thereby generating hydrogen peroxide [10,11]. The initial product formed is the respective imine, but this typically rapidly reacts with water to form a ketone or aldehyde and ammonia. The formation of the labile imine product intermediate is crucial for the chemo-enzymatic desymmetrization of chiral amines that involves an amine oxidase as biocatalyst [8]. A recent bioinformatic study further divided the flavoprotein amine oxidase superfamily into eight different subgroups based on substrate preference [12], with perhaps the most well-known subgroup being the monoamine oxidases (MAOs) (EC1.4.3.4). The human proteome contains two MAOs: MAO A and MAO B. These human MAOs play vital roles in the regulation of neurotransmitters and are linked with depression, obesity, cancer, and a plethora of other diseases [13–16]. As a consequence, specific MAO inhibitors are highly valued by the pharmaceutical industry. A fungal MAO, MAO-N from *Aspergillus niger*, has been thoroughly studied and engineered for its biocatalytic properties [17]. It has allowed the development of the above-mentioned biocatalytic procedure to prepare enantiopure amines, extremely useful building blocks for the pharma industry [8,18].

Clearly, MAOs have considerable biotechnological potential, and homologs are highly sought after for their potential use. Interestingly, most known, studied, and applied MAOs are from eukaryotic origin. Yet, bacterial genomes also harbor genes encoding (putative) MAOs. While the precise biological function of MAOs in prokaryotes is unknown, there are indications that they play a role in degradation pathways, thereby utilizing amines as a nitrogen source. A bacterial MAO from *Corynebacterium ammoniagenes*, was recently described which acts on typical mammalian MAO substrates [19]. Thus, bacteria form a potential source for new homologs. Such bacterial homologs may have an additional attractive feature when compared with eukaryotic MAOs: the expression in bacterial hosts provides easy access to these potential biocatalysts and enables the use of effective enzyme engineering approaches. Expression of human and mammalian MAOs has been shown to be extremely difficult in *Escherichia coli*. Currently, recombinant human MAO is produced in yeast. Thus, thermophilic bacteria, which are recognized for being exceptional sources of robust biocatalysts, form a promising source for thermophilic MAO homologs [20]. Herein, using the sequence of putrescine oxidase from *Rhodococcus erythropolis* (PuO$_{Rh}$) [21] as query, a thermostable MAO was discovered from a thermophilic *Thermoanaerobacterales* bacterium (MAO$_{Tb}$). Through elucidation of its crystal structure, biochemical characterization, and (pre-)steady-state kinetics, its biocatalytic potential has been explored and its striking structural resemblance with human MAO A has been exposed. These features make this newly discovered flavin-containing amine oxidase an attractive enzyme for future biotechnological exploitation.

Results

Identification

Using the protein sequence of PuO$_{Rh}$ (EC1.4.3.10), a PSI-BLAST search was performed on genomes of thermophilic bacteria. The structures of the best-scoring protein sequences were predicted using ColabFold [22]. A putative monoamine oxidase (MAO$_{Tb}$) from a *Thermoanaerobacterales* bacterium (GenBank: MBO2502335.1, 453 amino acids) showed a relatively high sequence identity (36%) when compared with putrescine oxidase. Structural comparison of its predicted model with the crystal structure of PuO$_{Rh}$ gave a root mean square deviation (RMSD) value of 1.3 Å. Further comparisons of the AlphaFold structure of the putative MAO were done using the Dali server [23]. Strikingly, the highest similarity was observed with human MAO A (EC1.4.3.4) with a RMSD value of only 0.9 Å. Also, when the sequences were compared, a relatively high sequence identity (37%) was observed between the bacterial and human proteins. A multiple sequence alignment using ESprit [24] of MAO$_{Tb}$ with human MAO A and human MAO B revealed the presence of some typical features of the human MAOs. It suggests that MAO$_{Tb}$ also contains (1) a conserved aromatic cage that forms part of the amine binding pocket, (2) a cysteine is found at a position to form a covalent 8α-(S-cysteinyl)-flavin linkage, and (3) several other conserved active site residues [25] (Fig. 1). Clearly, all these features hint to MAO$_{Tb}$ being a MAO. Nonetheless, there is a clear difference when compared to the human homologs; MAO$_{Tb}$ lacks the membrane-binding domain that is present in the human MAOs as C-terminal extension. This suggests that the bacterial enzyme may be a soluble protein which could make
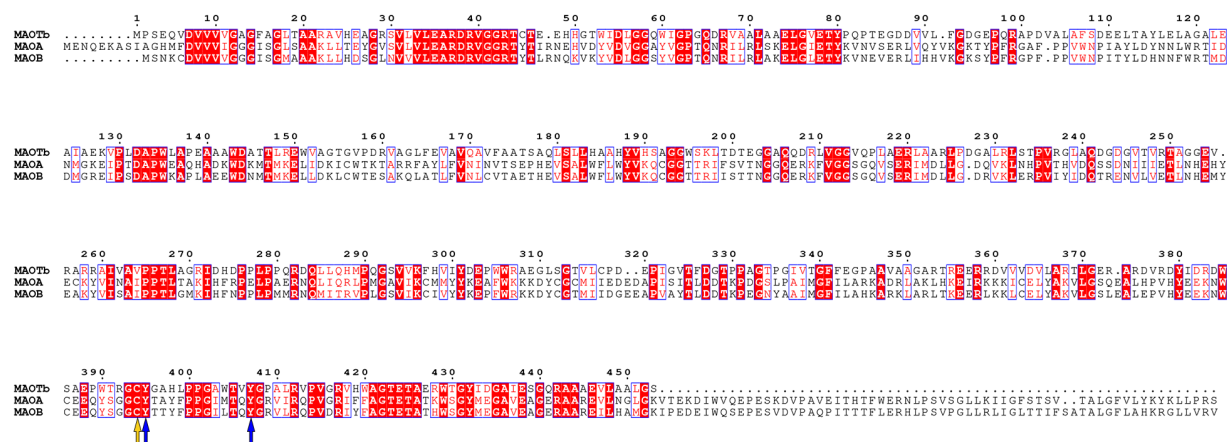
Fig. 1. Multiple sequence alignment of monoamine oxidase from *Thermoanaerobacterales* bacterium (MAO$_{Tb}$), MAO A, and MAO B generated with ESpript [24]. Conserved residues are shown with a red background. The conserved FAD-biding cysteine is marked with a yellow arrow and the aromatic cage with a blue arrow.

expression, purification, and application relatively easy when compared to the mammalian counterparts.

Expression, purification, and UV–vis absorbance characterization

The synthetic gene encoding MAO$_{Tb}$ was cloned into a pBAD vector for expression of the protein with a N-terminal His-tag. The recombinant protein was overexpressed in *E. coli* NEB10β and purified by affinity chromatography, resulting in a yellow-colored sample. It resulted in a yield of 75 mg purified protein per liter of culture. SDS/PAGE analysis showed that the purified protein could be obtained relatively pure after a single His-tag purification step, revealing a protein band of 51 kDa (the theoretical mass of the expressed protein is 49 kDa). A fluorescent band at the same position could be observed under UV light after a short incubation in 5% v/v acetic acid indicating the presence of a covalently bound flavin cofactor [26] (Fig. 2A). This is in line with the predicted presence of a cysteinyl-bound FAD cofactor. The UV–vis absorbance spectrum of MAO$_{Tb}$ showed two characteristic oxidized flavin absorbance bands with maxima at 462 nm and 380 nm. The A_{280}/A_{462} ratio of 10.9 showed that the enzyme was obtained mainly in its holo form and the molar extinction coefficient for MAO$_{Tb}$ ($\varepsilon_{462\ nm} = 12.7\ \mathrm{mM}^{-1}\ \mathrm{cm}^{-1}$) could be obtained by comparing its flavin absorbance spectrum with that upon SDS-induced unfolding (Fig. 2B). Dynamic light scattering suggests that MAO$_{Tb}$ exists as a native dimer (73 kDa), exhibiting even more similarity to human and other eukaryotic MAOs [27] (Fig. 3A). This result was confirmed by gel filtration,

performed in 50 mM KP$_i$ pH 7.5 buffer, which gave an elution volume of 70 mL corresponding to 90–100 kDa (Fig. 3B).

Biochemical characterization

The thermostability of MAO$_{Tb}$ was explored using the ThermoFAD assay, which reported a T_m of 73 °C at pH 5.5, with a preference for acidic conditions and notable resilience toward the probed solvents (Table 1), while aggregation was observed at acidic pH's of below 5. The addition of up to 10% DMSO or MeOH resulted in a marginal reduction in its melting temperature (reduction of ≤6 °C). To probe the substrate specificity of MAO$_{Tb}$, an activity assay using the consolidated HRP-coupled protocol used for MAO enzymes [28] was performed. Initially, some typical substrates of MAO enzymes such as benzylamine, kynuramine, MMTP (1-methyl-4-(1-methyl-1H-pyrrol-2-yl)-1,2,3,6-tetrahydropyridine), and phenylethylamine were screened, followed by some substrates of the polyamine oxidase family including putrescine, spermidine, and spermine. All substrates were tested at a concentration of 4.0 mM. As shown in Table 2, the activity was barely detected. Due to the lack of activity observed so far, the structural comparison of the AlphaFold model of MAO$_{Tb}$ by the Dali server was revisited. The search reported a high structural similarity with cyclohexylamine oxidase from *Brevibacterium oxydans* (CHAO, PDB code 4I58), implying that the enzyme may exhibit a similar substrate scope. Cyclohexylamine and *n*-hexylamine were therefore tested, resulting in MAO$_{Tb}$ being inactive on the former but highly active on *n*-hexylamine (k_{obs} 14 s^{-1}).

(A)

(B)
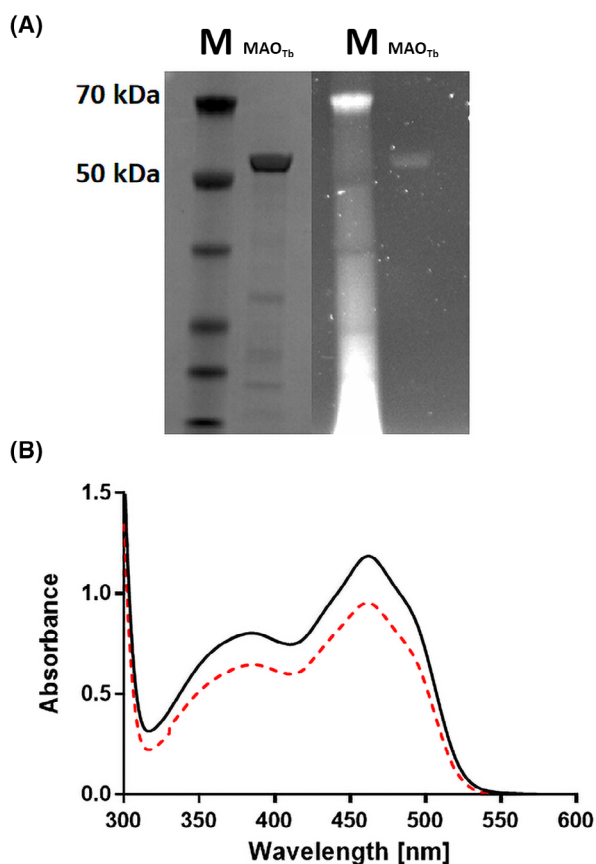
Fig. 2. (A) SDS/PAGE gel (4%–12%) of His-tagged purified monoamine oxidase from *Thermoanaerobacterales* bacterium (MAO$_{Tb}$) observed around 50 kDa. The left image shows the gel Coomassie stained and the right one acetic acid (5% v/v) stained for 5 min under UV light. The M stands for the molecular weight markers and his-tag-purified protein is marked with MAO$_{Tb}$ (B) UV–vis absorbance spectra of 90 µM MAO$_{Tb}$, before (solid black line) and after treatment with 0.1% SDS (broken red line), in 50 mM KP$_i$ pH 7.5.

Accordingly, an extended analysis of other aliphatic monoamines was done and an increasing activity proportionally to the chain length from *n*-butylamine to *n*-heptylamine was observed (Table 2). *n*-Octylamine and *n*-nonylamine proved substrates of MAO$_{Tb}$ although accurate kinetic analyses were impossible due to limited solubility. To investigate MAO$_{Tb}$ activity on secondary and tertiary amines, methyl- and dimethyl-hexylamine were tested which were active though at about threefold and 10-fold less than *n*-hexylamine, respectively. All these data indicate that MAO$_{Tb}$ is a flavin-dependent amine oxidase with a substrate specificity for long aliphatic monoamines, whereas is barely active or inactive on cyclic aliphatic and aromatic monoamines.

The thermal stability for MAO$_{Tb}$ was also tested by measuring the enzymatic activity at different temperatures (Fig. 4A). The activity was tested by performing the HRP-coupled assay in 50 mM HEPES/NaOH buffer pH 7.5 with 1.0 mM *n*-heptylamine and increasing the temperature from 25 to 85 °C. The activity of MAO$_{Tb}$ increases with temperatures, reaching the maximum at 75 °C, and it drops drastically at 85 °C.

Next, the effect of ionic strength on MAO$_{Tb}$ activity was tested by performing the HRP-coupled assay in the same buffer used for substrate screening (50 mM HEPES/NaOH buffer pH 7.5) and adding increasing concentration of different salts (Fig. 4B) with 1.0 mM *n*-heptylamine. MAO$_{Tb}$ activity drops to less than 25% at 10 mM of bivalent cations (MgCl$_2$, CaCl$_2$, and MnCl$_2$) and is almost undetectable at 100 mM. The effect of monovalent cations (NaCl and KCl) is less dramatic with little or no drop in activity at 10 mM, while retaining almost 50% and 25% of activity at 50 mM and 200 mM salt, respectively. Similarly, a screening of different buffer conditions to probe the pH dependence of MAO$_{Tb}$ activity by measuring the k_{obs} with 1 mM *n*-heptylamine at 25 °C was performed. The optimal pH curve is bell-shaped centered at 7.5–8.5 in 50 mM HEPES/NaOH (Fig. 4C). However, in this pH range MAO$_{Tb}$ activity is maximal also with other buffers and k_{obs} values are only slightly lower probably due to differences in ionic strength that was above shown to exert an effect.

Steady-state kinetics

To determine the steady-state kinetic parameters of MAO$_{Tb}$ with the substrates displaying k_{obs} values equal or higher than 0.5 s^{-1} (Table 2), the enzymatic activity was followed by the consumption of oxygen during time using an Oxygraph plus system (Hansatech Instruments Ltd., Pentney, UK). This approach requires larger amounts of enzyme than the HRP-coupled assay but provides a direct method to probe MAO$_{Tb}$ activity. Although the optimal pH curve showed the highest k_{obs} value in HEPES buffer, these experiments were performed in 50 mM potassium phosphate at pH 7.5 because MAO$_{Tb}$ showed the best gel filtration profile and homogeneity properties in these conditions (Fig. 3B) and this buffer is more convenient for biocatalytic applications. Table 3 reports the steady-state parameters and Fig. 5 shows the data fitted to the Michaelis–Menten equation. *n*-Heptylamine is the best substrate ($k_{cat}/K_M = 25.5$ mM^{-1} s^{-1}), followed by *n*-hexylamine that features a 10-fold lower catalytic efficiency. Methyl-hexylamine and *n*-pentylamine are also good substrates with about half of the k_{cat}/K_M value

(A)

	Radius (nm)	%Pd	Mw-R (kDa)	%Intensity	%Mass
Peak 1	3.731	11.9	73	85.8	100.0
Peak 2	115.508	14.4	225570	7.8	0.0
Peak 3	3815.910	32.6	807984000	6.4	0.0

(B)
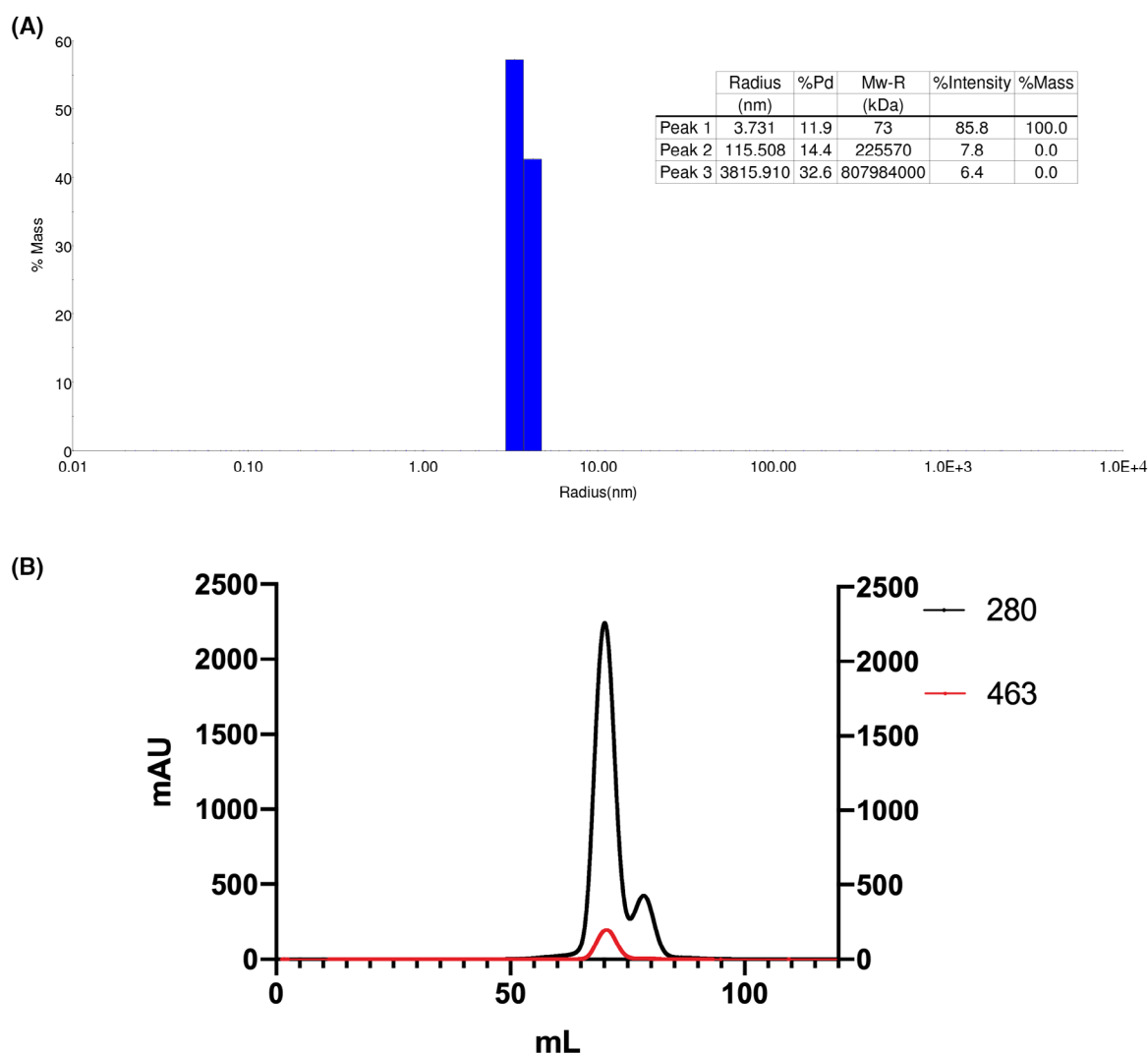
Fig. 3. (A) Dynamic light scattering analysis of monoamine oxidase from *Thermoanaerobacterales* bacterium (MAO$_{Tb}$). The inset shows the predicted mass. (B) Chromatogram of MAO$_{Tb}$ upon size-exclusion chromatography in 50 mM potassium phosphate buffer pH 7.5, using Superdex200 16/60 and monitoring absorbance at 280 and 463 nm (black and red respectively).

with respect to *n*-hexylamine. *n*-Butylamine is a much poorer substrate, as shown by the high K_M value and the Michaelis–Menten profile (Fig. 5A). Determination of the steady-state parameters with dimethylhexylamine was hampered by the low solubility of the compounds at the concentrations required to reach the k_{cat} values at the plateau.

Presteady-state kinetics

Mixing MAO$_{Tb}$ anaerobically with substrate resulted in a rapid decrease in flavin absorbance, yielding a fully reduced flavin spectrum within 1 s. The formation of fully reduced MAO$_{Tb}$ indicates that flavin reduction is effectively an irreversible process. Deconvolution of the spectral data revealed that reduction proceeds via just one kinetic event, without any detectable intermediate. This is in line with the observed kinetic behavior of human MAO A and MAO B, and may hint to a hydride transfer mechanism. Using a range of *n*-hexylamine concentrations allowed determination of the maximum rate of reduction (k_{red}) of $14.1 \pm 1.1 \text{ s}^{-1}$, together with a K_d of 0.80 mM (Fig. 6A). Using substrate-reduced MAO$_{Tb}$, the rate of reoxidation was monitored by mixing with aerobic buffer. Again, a rapid and single kinetic event was observed, now resulting in fully oxidized MAO$_{Tb}$ (Fig. 6B). The observed rate of reoxidation (14.6 s^{-1})

Table 1. Thermal stabilities of monoamine oxidase from *Thermoanaerobacterales* bacterium (MAO$_{Tb}$) in different buffers and conditions.

Buffer (50 mm)	Melting temperature (°C)
Citrate buffer pH 5.0	71
Citrate buffer pH 5.5	73
KPi pH 6.0	72
KPi pH 6.5	72
KPi pH 7.0	69
KPi pH 7.5	65
TRIS–HCl pH 8.0	63
TRIS–HCl pH 8.5	62
TRIS–HCl pH 9.0	58
5% DMSO, KPi pH 7.5	63
10% DMSO, KPi pH 7.5	60
5% MeOH, KPi pH 7.5	63
10% MeOH, KPi pH 7.5	59

is underestimated when compared with atmospheric aerobic conditions as aerobic buffer was mixed 1:1 in the stopped-flow instruments with anaerobic enzyme solution. Thus, with oxidases typically having no apparent affinity constant for dioxygen, the rate of reoxidation at atmospheric conditions is around 30 s^{-1}. Clearly, MAO$_{Tb}$ acts as a *bona fide* flavoprotein oxidase as it is efficient in using dioxygen as electron acceptor. Nevertheless, the K_M value for oxygen could not be determined. When measuring hexylamine oxidase activity at dioxygen concentrations up to 240 μM, there is a nearly linear dependence between activity and dioxygen concentration (Fig. 6C). It shows that it has a poor apparent affinity toward dioxygen as electron acceptor.
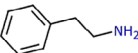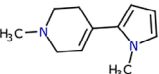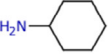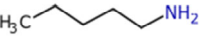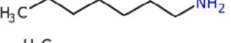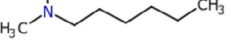
X-ray crystallography

The crystal structure of MAO$_{Tb}$ was determined at 1.5 Å resolution by molecular replacement using the AlphaFold model (Fig. 7 and Table 4). Two protein molecules are contained in the asymmetric unit which form a dimer (Fig. 7A) whose monomer-monomer interface area (1584 Å^2) corresponds to 24% of the total protein surface. This dimeric architecture is likely to represent the oligomeric form of the enzyme in solution as observed in the gel filtration profile (Fig. 3B). Moreover, the dimer is the same as that found in the human MAO B structure, which features a monomer-monomer interface of 2095 Å^2 (corresponding to 15% of the total protein surface) [29]. The RMSD for each pairwise of C$_\alpha$ atoms of chains A and B is 0.47 Å; hence, hereafter, chain A will be referred to for the purpose of structural description. Out of the 452 residues of MAO$_{Tb}$, only the first four N-terminal

amino acids in either chain lack clear electron density and were hence omitted from the coordinate file of the refined structure. In each monomer, the FAD cofactor is covalently bound to Cys394 (Fig. 8) as inferred from SDS/PAGE analysis (Fig. 2A) and predicted also by the sequence alignment of the homologous human MAO A and MAO B (Fig. 1).

The MAO$_{Tb}$ active site consists of a cavity that originates from the flavin ring and has approximately a constant diameter until residues 199–201, then broadens reaching the protein surface (Fig. 7B). This part includes a side appendix where a magnesium ion is bound coordinated by five water molecules. Indeed, magnesium was present in the crystallization solution and divalent cations exert an inhibitory effect on enzyme activity (Fig. 4B). The total volume of the cavity is about 725 Å^3 calculated with Voss Volume Voxelator [30]. The core of the active site in front of the flavin is characterized by two tyrosine residues, Tyr432 and Tyr395, which form the 'aromatic cage' typically found in FAD-dependent amine oxidases, including the human MAOs. Other fully conserved elements of MAO$_{Tb}$ with respect to human MAOs include the presence of a *cis* peptide bond between Tyr395 of the aromatic sandwich and Cys394 (involved in the covalent bond to FAD), and a tyrosine residue (Tyr188) with its hydroxyl group pointing toward the cage formed by the flavin and the aromatic sandwich (Fig. 7B). Moreover, similarly to human MAOs the isoalloxazine ring of the cofactor has a nonplanar conformation with its N5 atom H-bonded to a water molecule stabilized by the conserved lysine residue (Lys296), whose function in dioxygen binding during FAD reoxidation was demonstrated [31].

While the core of the active site around the flavin cofactor is highly similar to human MAOs, differences arise at the bottleneck of the cavity (Fig. 7B), which nevertheless also MAO A and MAO B feature distinctive elements. Besides Val172 (Asn181 in MAO A and Cys172 in MAO B), the pair Thr199/Val324 correspond to the gating residues that play a key role in ligand binding specificity between the human enzymes (Phe208/Ile335 in MAO A and Ile199/Tyr326 in MAO B). Although the Dali search identified human MAO A (PDB code 2Z5X) as the most similar structure (RMSD = 1.3 Å), these residues in MAO$_{Tb}$ highlight a midway situation with respect to the human enzymes. The Thr/Val pair in MAO$_{Tb}$ are both small-size residues which creates a wider access to the active site. Even more divergent is the conformation of the polypeptide segment (residues 83–124 in MAO$_{Tb}$) on the protein surface which folds into a loop followed by a long α-helix delimiting the entrance of the cavity

Table 2. Substrate screening of monoamine oxidase from *Thermoanaerobacterales* bacterium (MAO$_{Tb}$) based on HRP-coupled assay at fixed concentration of substrate of 4.0 mM. As described in the Methods section, the measurements were performed in 50 mM HEPES/NaOH buffer pH 7.5 (25 °C). All assays were carried out in duplicate.

Compound	Chemical structure	k_{obs} (s^{-1})
Benzylamine		0.04 ± 0.01
Kynuramine		0.04 ± 0.01
Phenylethylamine		0
MMTP		0
Putrescine		0.03 ± 0.01
Spermidine		0.1 ± 0.02
Spermine		0
Methylbenzylamine		0
Cyclobutylamine		0
Cyclohexylamine		0
n-Butylamine		0.5 ± 0.1
n-Pentylamine		1.2 ± 0.5
n-Hexylamine		14.1 ± 1.9
Methyl-hexylamine		4.2 ± 0.4
n-Heptylamine		64.4 ± 0.9
Dimethylhexylamine		1.2 ± 0.1
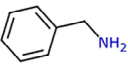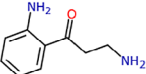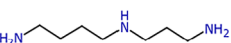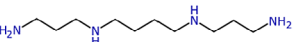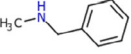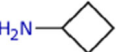
(Fig. 9A). This motif is found also in human MAO A though with a different layout, mainly in the loop that in MAO$_{Tb}$ has a more folded conformation leaving more space to the entrance of the cavity. Moreover, analysis of the surface electrostatic potential revealed that MAO$_{Tb}$ is particularly negatively charged at the base of the dimer that includes the substrate binding domain (Fig. 7C), which may favor the binding of the positively charged amine substrates. This aspect is completely different from the human MAOs which display a more heterogenous charge distribution and more hydrophobic character in this portion of the

dimer where the C-terminal membrane helices are located.

An even more divergent conformation of the α-helix/loop motif can be found in a recently identified bacterial MAO from *C. ammoniagenes* (MAO$_{ca}$, PDB code 8EEI, RMSD = 1.1 Å) [19], where the α-helix is highly deviated with respect to MAO$_{Tb}$ and human MAO A and the loop is shorter (Fig. 9A). Interestingly, MAO$_{ca}$ has the conserved lysine residue interacting with FAD while the aromatic sandwich flanking the flavin ring is partly conserved with a tryptophan and a cysteine replacing Tyr395 and Tyr432 of MAO$_{Tb}$,
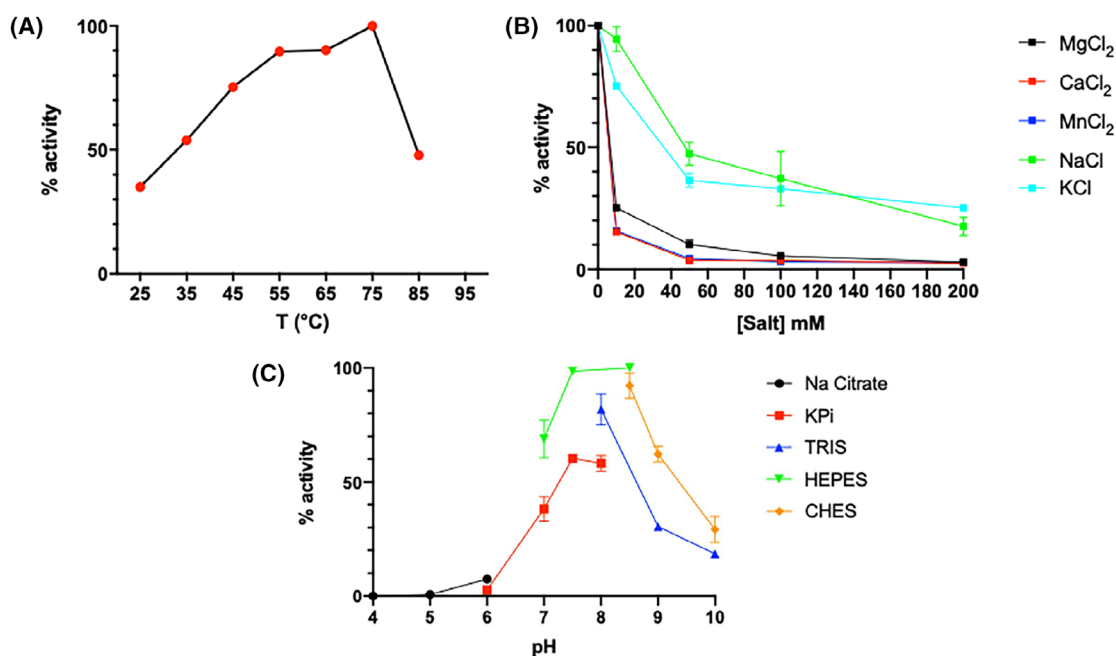
Fig. 4. Effect of temperature, salt, and pH on the activity of monoamine oxidase from *Thermoanaerobacterales* bacterium (MAO$_{Tb}$). For measuring activity, 1.0 mM *n*-heptylamine was used. All measurements were performed in duplicate. (A) Effect temperature (from 25 to 85 °C) on MAO$_{Tb}$ activity in HEPES buffer pH 7.5. (B) Effect of different mono- and divalent cations (from 0 to 200 mM) on the activity of MAO$_{Tb}$ in HEPES buffer pH 7.5, at 25 °C. (C) Effect pH on MAO$_{Tb}$ activity, at 25 °C. Different buffer types (indicated in different colors) were used to cover a wide range of pH values. Error bars indicate SD and all points were taken in duplicates ($n = 2$).

Table 3. Steady state kinetic parameters of MAO$_{Tb}$ with aliphatic monoamines. As described in the Materials and methods section, the measurements were performed in 50 mM potassium phosphate buffer pH 7.5 (25 °C) by following oxygen consumption. All assays were carried out in duplicate.

Substrate		k_{cat} (s^{-1})	K_M (mM)	k_{cat}/K_M (mM^{-1}·s^{-1})
n-Butylamine		1.8 ± 0.2	40.1 ± 9.1	0.05
n-Pentylamine		2.9 ± 0.2	3.3 ± 0.8	0.9
n-Hexylamine		9.9 ± 0.5	4.1 ± 0.6	2.4
n-Heptylamine		25.5 ± 0.9	1.0 ± 0.2	25.5
Methyl hexylamine		3.2 ± 0.1	2.9 ± 0.4	1.1

respectively. The comparative structural analysis was extended also to *Aspergillus niger* MAO (MAO N, PDB code 2VVM), which is known to feature the conserved lysine residue mentioned above and a partly conserved aromatic sandwich in which the classical Tyr/Tyr pair is replaced by Phe/Trp. Nevertheless, the MAO N dimer is different with respect to that found in human MAOs and MAO$_{Tb}$, and also the overall structural homology is lower (RMSD 2.4 Å). Interestingly, both in MAO$_{ca}$

and in MAO N, the FAD cofactor is not covalently bound and both enzymes feature a Trp residue corresponding to Tyr188 found in human MAOs/MAO$_{Tb}$ (Fig. 9A). The Dali search returned two bacterial amine oxidases with significant overall structural similarity, namely putrescine oxidase from *R. erythropolis* (PuO$_{Rh}$, PDB code 2YG4) and cyclohexylamine oxidase from *B. oxydans* (CHAO, PDB code 4I58). In both cases, the oligomeric organization does not follow the dimeric
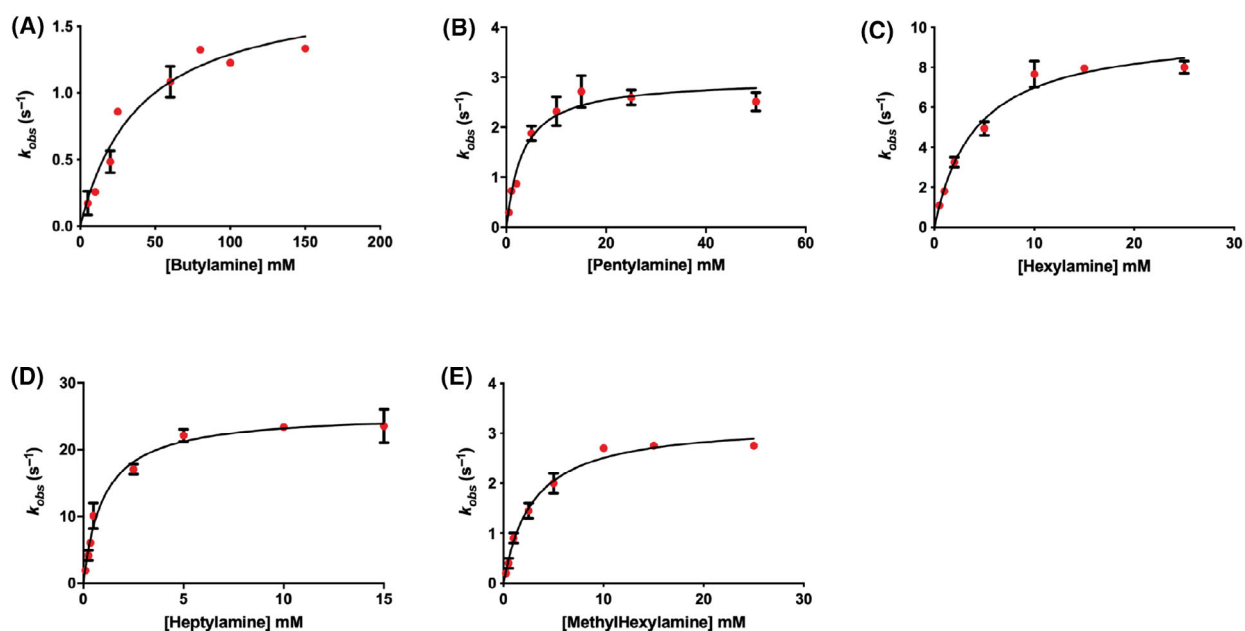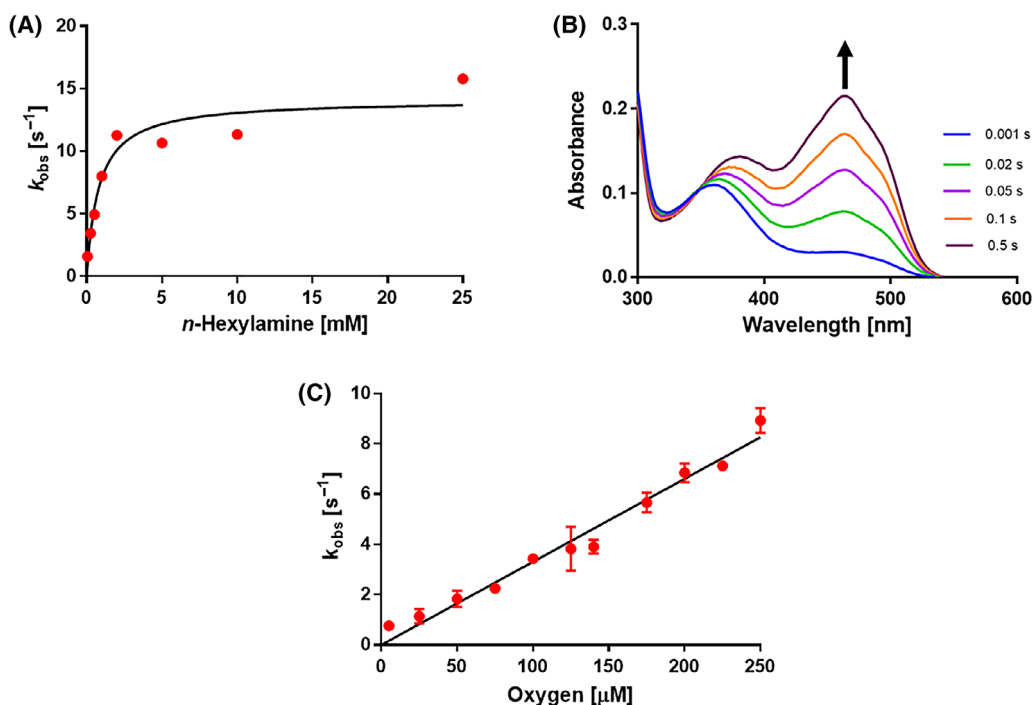
Fig. 5. Michaelis–Menten fitted curves of monoamine oxidase from *Thermoanaerobacterales* bacterium (MAO$_{Tb}$) with the aliphatic monoamine substrates performed at the Oxygraph in 50 mM potassium phosphate buffer pH 7.5 (25 °C). All points for the different concentration of substrates were performed in duplicate. (A) *n*-butylamine. (B) *n*-pentylamine. (C) *n*-hexylamine. (D) *n*-heptylamine. (E) methyl hexylamine. Error bars indicate SD, and all points were taken in triplicates (*n* = 3).

structure of MAO$_{Tb}$, but the overall fold of the monomer is highly similar (Fig. 9B), including the α-helix/loop motif wrapping the entrance of the active site cavity (RMSD 1.6 Å and 1.9 Å with respect to PuO$_{Rh}$ and CHAO, respectively). Being FAD-dependent amine oxidases, both PuO$_{Rh}$ and CHAO contain the lysine interacting with the flavin edge, whereas the aromatic sandwich is only partly conserved with Tyr395 and Tyr432 of MAO$_{Tb}$ replaced respectively by Pro422 in CHAO and His432 in PuO$_{Rh}$ (Fig. 9B). Moreover, Tyr188 of MAO$_{Tb}$ is conserved in CHAO, whereas it is replaced by a methionine in PuO$_{Rh}$.

Discussion

Herein, utilizing the sequence of PuO$_{Rh}$ (ABY74497.1), a novel thermostable MAO, MAO$_{Tb}$ was described from a *Thermoanaerobacterales* bacterium. The enzyme is endowed with favorable characteristics as its yield per liter culture is 70 mg, it is easily storable for up to 2 months at 4 °C and has a melting temperature of 73 °C at pH 5.5. Even though MAO$_{Tb}$ was found in an obligated anaerobic bacteria order [32], its presteady-state kinetics showed that the enzyme can act as a true flavoprotein oxidase as it is efficient in using dioxygen as electron acceptor at atmospheric conditions.

Interestingly, the affinity for molecular oxygen was found to be very poor (high K_M value). This suggests that under natural conditions, it utilizes an alternative electron acceptor, acting as an amine dehydrogenase. The poor efficiency as oxidase at low oxygen concentrations suggests that it is not used as enzyme for scavenging dioxygen. Structural elucidation of the enzyme with a resolution of 1.5 Å showed high structural similarity with human MAO A and MAO B. All three enzymes form dimers, have a conserved tyrosine aromatic cage, FAD-binding cysteine, and a conserved lysine residue stabilizing the nonplanar conformation of the cofactor with its N5 atom interacting with water for FAD reoxidation by dioxygen. Despite this high similarity, MAO$_{Tb}$ differs from the human MAOs mainly by lacking the C-terminal membrane-binding α-helix and having a more open and wider accessible active site due to differences in gating residues and a surface polypeptide segment. This in turn can explain the difference in substrate scope, as MAO$_{Tb}$ prefers aliphatic monoamines showing high catalytic rates on both *n*-hexylamine and *n*-heptylamine, with only residual activity on cyclic monoamines. Everything considered, MAO$_{Tb}$ presents itself as a robust candidate for the conversion of fishy odor aliphatic amines to more odor-neutral products. The covalent flavoprotein oxidase also has potential

Fig. 6. (A) Michaelis–Menten fitted plot of reduction rates of monoamine oxidase from *Thermoanaerobacterales* bacterium (MAO$_{Tb}$) with different concentrations of *n*-hexylamine. (B) Some selected UV–vis absorbance spectra when 40 μM anaerobically reduced MAO$_{Tb}$ is mixed (1:1) with 240 μM molecular oxygen in 50 mM KP$_i$ (pH 7.5). The time at which each spectrum was collected is indicated in seconds. (C) Oxidase activity with hexylamine (40 mM) at various oxygen concentrations in 50 mM KP$_i$, pH 7.5 (25 °C). Error bars indicate SD, and all points were taken in duplicates (*n* = 2).

to serve as an alternative for the difficulty to produce mammalian MAOs for pharma-related research. The elucidated crystal structure can be of help when the enzyme needs to be engineered for a specific application.

Materials and methods

Chemicals and materials

Ni-Sepharose 6 Fast Flow for protein purification and HiLoad Superdex 200 16/60 column for size-exclusion chromatography runs were obtained from Cytiva (Marlborough, MA, USA). *n*-butylamine, *n*-pentylamine, *n*-heptylamine were obtained from Thermo Fisher Scientific (Waltham, MA, USA). All other chemicals were obtained from Sigma-Aldrich (Merck, St. Louis, MO, USA).

Genome mining

To identify putative MAO homologs in thermophilic bacteria, the PSI-BLAST tool of the National Center for Biotechnology Information (NCBI) was utilized with the sequence of PuO$_{Rh}$ (ABY74497.1) as input. Sequence alignments were performed using ESpript [24]. Promising

sequences were chosen and their structures were predicted using the online AlphaFold tool ColabFold [22,33]. Using the PyMOL software [34], AlphaFold structures were aligned with crystal structures of MAO A, MAO B, and PuO$_{Rh}$. Further structural comparisons were done using the Dali protein structure comparison server [23].

Cloning and transformation

The synthetic gene for expression of MAO$_{Tb}$ in *E. coli* with *Bsa*1 sites at its 5′- and 3′-termini was ordered from Twist Biosciences (South San Francisco, CA, USA). The synthetic gene was cloned into a pBAD-His vector using the Golden Gate methodology [35]. Heat shock transformation was carried out by mixing 2 μL of resulting PCR product with 40 μL CaCl$_2$ competent *E. coli* NEB10β cells. The mixture was kept on ice for 30 min after which the heat shock was performed at 42 °C for 45 s. The cells were cooled for 5 min on ice and mixed with 250 μL LB-media for a 1 h recovery period at 37 °C. Subsequently, 50 μL of the mixture was plated on LB-agar plates containing 50 μg/mL ampicillin (amp) and left overnight in a 37 °C stove. Obtained colonies were grown in LB containing 50 μg/mL amp at 37 °C overnight. After which plasmid isolation could be performed and cloning was verified with sequencing.

(A)

(B)

(C)
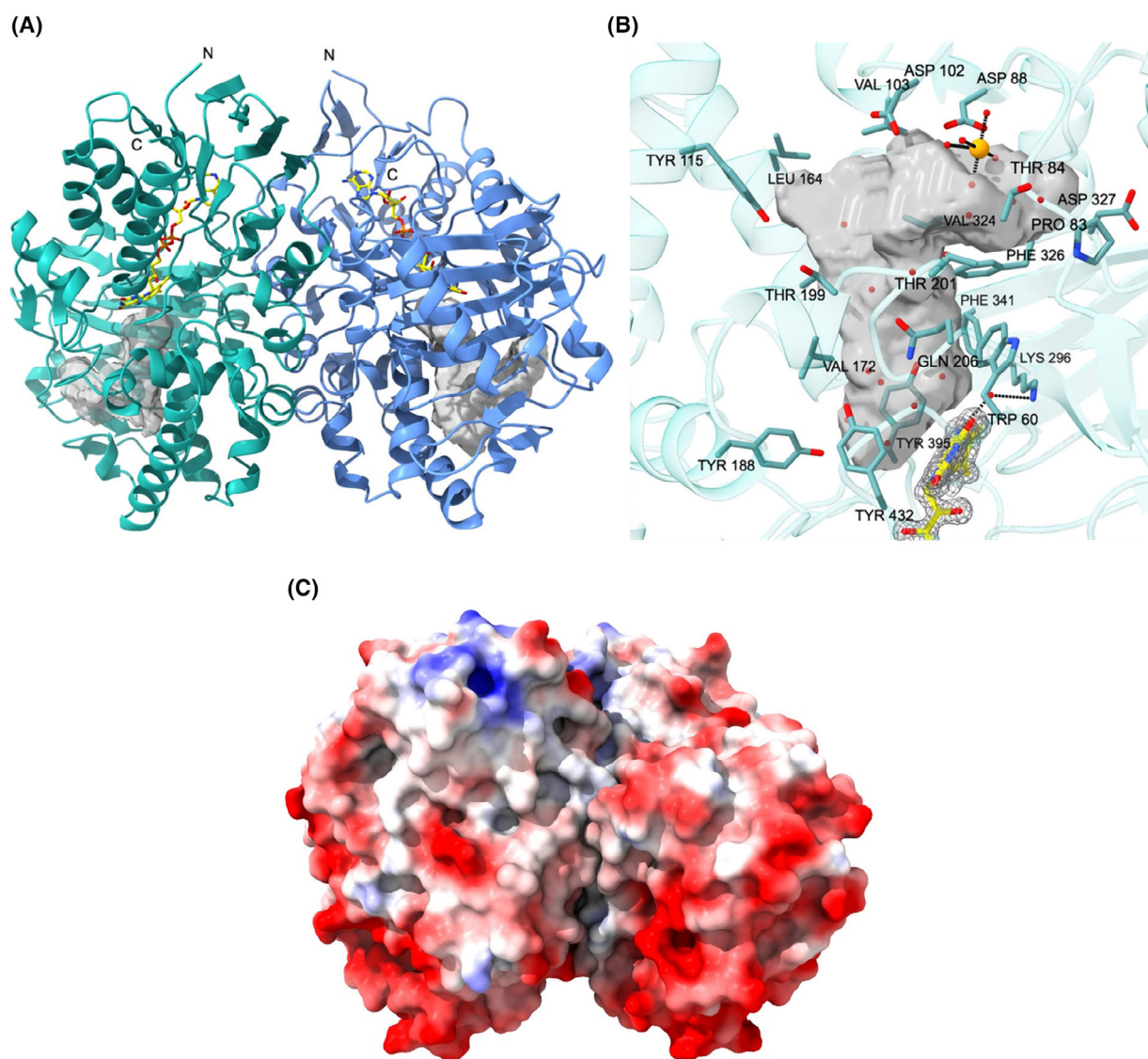
Fig. 7. Three-dimensional structure of monoamine oxidase from *Thermoanaerobacterales* bacterium (MAO$_{Tb}$). (A) Ribbon diagram of the overall MAO$_{Tb}$ dimeric structure (chain A and B are colored in light sea green and cornflower blue, respectively). In each monomer, the FAD cofactor bound (represented with carbon, oxygen, nitrogen, and phosphorus atoms in yellow, red, blue, and magenta, respectively), and the active site cavity (drawn as semitransparent surface) are shown. (B) Zoomed view of the MAO$_{Tb}$ active site (the molecule is rotated of about 180° with respect to the representation in (A)). Active site residues shown as sticks (represented with carbon, oxygen, nitrogen atoms in light sea green, red, and blue, respectively). A magnesium ion and water molecules are represented as orange and red spheres, respectively. Hydrogen bonds are shown as dashed lines. Refined 2F$_o$-F$_c$ electron density drawn is drawn as gray chicken wire representation contoured at 1.5 σ for the FAD cofactor. (C) Surface electrostatic potential of MAO$_{Tb}$ dimer, showing the positively and negatively charged patches in blue and red, respectively. The structure is oriented as in (A). Structures were visualized using USCF ChimeraX [42].

Protein expression, purification, and characterization

For expression of MAO$_{Tb}$, overnight cultures grown in 5 mL LB containing 50 µg/mL amp at 37 °C were resuspended into 200 mL Terrific Broth medium supplemented with 50 µg/mL amp and incubated at 37 °C in a non-baffled flask. Once an OD$_{600}$ of ~0.6 was reached, the culture was induced by supplementing a final concentration of 0.02% L-arabinose. After which the culture was incubated at 24 °C. After ~16 h, the cells were pelleted by centrifuging (3700 r.p.m., 15 min, 4 °C) and stored at -20 °C.

For purification, cell pellets were resuspended into 20 mL lysis buffer (50 mM TRIS–HCl, 150 mM NaCl, pH

Table 4. Data collection and refinement statistics for monoamine oxidase from *Thermoanaerobacterales* bacterium (MAO_{Tb}).

PDB code	8P84
Space group	P $2_1 2_1 2_1$
Unit cell dimensions (Å)	$a = 67.93$, $b = 94.17$, $c = 127.28$
Resolution (Å)	1.5 Å
R_{merge}[a,b]	0.054 (1.158)
$CC_{1/2}$[b,c]	0.999 (0.689)
Completeness[b] (%)	100.0 (99.9)
Redundancy[b]	6.7 (6.9)
I/σ[b]	17.6 (1.7)
Unique reflections[b]	131 032 (6419)
N° of protein/FAD atoms	6722/2 × 53
N° of water atoms	676
N° of Mg/glycerol atoms	3/6
Average B value (Å^2)	19.0
Ramachandran outliers	0
Clash scores	2
R_{cryst}[d] (%)	15.9
R_{free}[d] (%)	18.5
RMSD bond length (Å)	0.014
RMSD bond angles (°)	1.8

[a]$R_{merge} = \sum |I_i - <I>| / \sum I_i$, where I_i is the intensity of ith observation and $<I>$ is the mean intensity of the reflection; [b]Values in parentheses are for reflections in the highest resolution shell; [c]A cut-off criterion for resolution limits was applied on the basis of the mean intensity correlation coefficient of half-subsets of each dataset ($CC_{1/2}$); [d]$R_{cryst} = \sum |F_{obs} - F_{calc}| / \sum |F_{obs}|$ where F_{obs} and F_{calc} are the observed and calculated structure factor amplitudes, respectively. R_{cryst} and R_{free} were calculated using the working and test (randomly chosen reflections) sets, respectively; RMSD, root mean square deviation.

8.0) and disrupted by sonication (5 s on, 7 s off, 70% amplitude for 10 min). The supernatant was harvested by centrifuging at 11 000 r.p.m. for 50 min at 4 °C and loaded onto gravity columns containing 2 mL lysis buffer equilibrated Ni-Sepharose. The column was incubated at 4 °C while rotating for 30 min. Subsequently, the column was washed with three column volumes of lysis buffer and 3 column volumes of wash buffer (50 mM TRIS–HCl, 150 mM NaCl, 20 mM imidazole, pH 8.0). MAO_{Tb} was eluted of the column by using 3.5 mL elution buffer (50 mM TRIS–HCl, 150 mM NaCl, 500 mM imidazole, pH 8.0). Using a PD10 buffer exchange column, the elution buffer was exchanged for 50 mM KP_i (pH 7.5) buffer, which was used as storage buffer. For crystallization experiments, the protein was gel-filtered using HiLoad Superdex 200 16/60 column (GE Healthcare, Chicago, IL, USA) equilibrated with 50 mM KP_i (pH 7.5) buffer using a ÄKTA pure™ (Cytiva, Marlborough, MA, USA).

MAO_{Tb} could be stored at 4 °C for up to 2 months without loss of activity. Concentrations were determined using its 462 nm extinction coefficient, which was
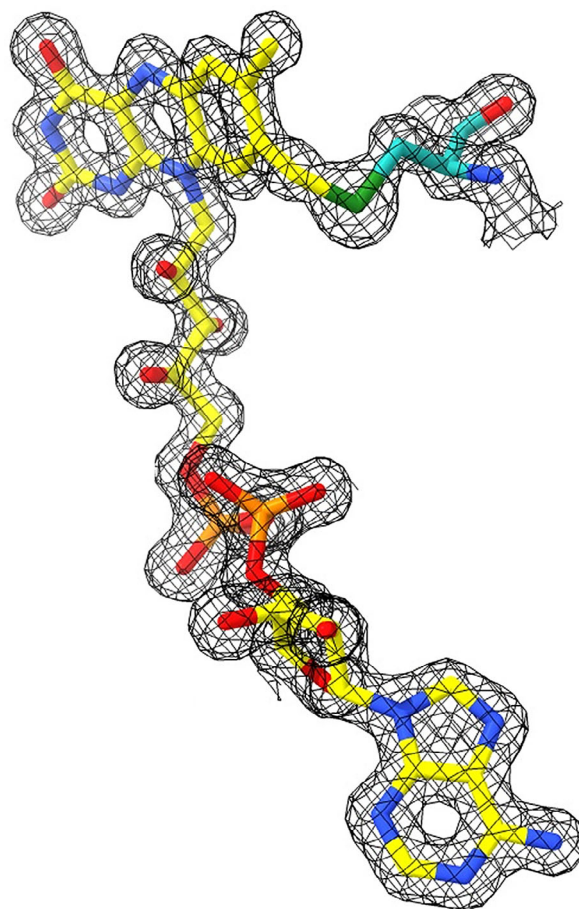

Fig. 8. Cys-FAD refined $2F_o$-F_c electron density contoured at 1.5 σ. The FAD part is shown with carbon, oxygen, nitrogen, and phosphorus atoms in yellow, red, blue, and magenta, respectively. The covalently linked Cys394 is represented with carbon, oxygen, nitrogen, and sulfur atoms in light sea green, red, blue, and green, respectively. Structure was visualized using USCF ChimeraX [42].

determined by comparing its UV–vis absorption before and after denaturation with 0.1% SDS, using a JASCO V-660 spectrophotometer (Hachioji, Tokyo, Japan).

The oligomeric state of MAO_{Tb} was determined by dynamic light scattering. For this, a 2.0 µL sample was analyzed in a DynaPro NanoStar instrument (Wyatt Technology, Santa Barbara, CA, USA) and data analysis was performed using the DYNAMICS software.

The melting temperature of MAO_{Tb} was determined in duplicates using the ThermoFAD assay [36]. One hundred micromolar enzyme in 50 mM KP_i (pH 7.5) was diluted fivefold in different buffers with different pH values, ranging from pH 5 to pH 9 or different solvent concentrations. The assay was measured starting from 20 to 99 °C with steps of 1 °C/30 s in a RT-PCR thermocycler (CFX96, Bio-Rad, Hercules, CA, USA).
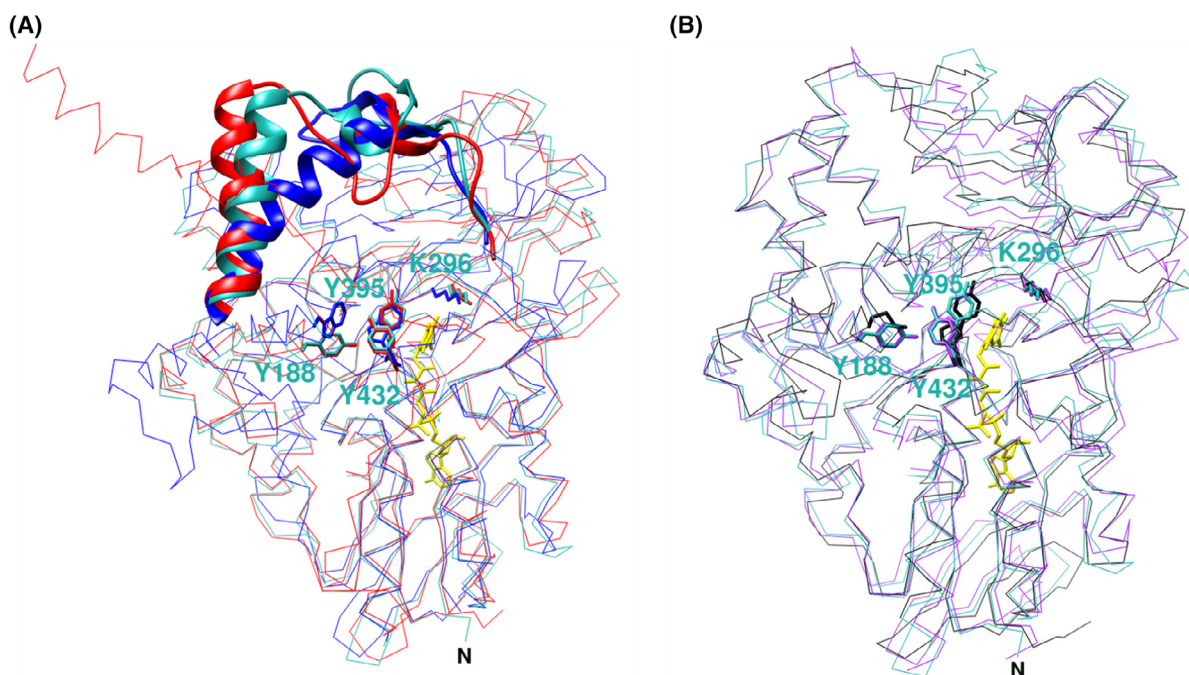
Fig. 9. Comparison of monoamine oxidase from *Thermoanaerobacterales* bacterium (MAO$_{Tb}$) structure with other FAD-dependent amine oxidases that display structural similarities. (A) Superposition of the C_α trace of MAO$_{Tb}$ (light sea green) with human MAO A and MAO$_{ca}$ colored in red and blue, respectively. The loops of MAO$_{Tb}$, human MAO A and MAO$_{ca}$ (residues 83–124, 91–134, and 82–118, respectively) delimiting the cavity entrance are highlighted as cartoons. Residues in the core of the active site (numbering of MAO$_{Tb}$ is shown) are drawn as sticks colored according to the C_α trace. FAD is in yellow. The *N* terminus of MAO$_{Tb}$ is indicated by '*N*' (the C terminus of the protein is on the back and for the sake of clarity it was not reported). (B) Superposition of the C_α trace of MAO$_{Tb}$ (light sea green) with putrescine oxidase from *Rhodococcus erythropolis* (PuO$_{Rh}$) and cyclohexylamine oxidase from *Brevibacterium oxydans* (CHAO) colored in black and purple, respectively. As in panel (A), key residues in the active site are shown. Structures were visualized using USCF Chimera [41].

Activity assays and steady-state kinetics

Activity assays were carried out by the horse radish peroxidase (HRP)-coupled assay in 50 mM HEPES/NaOH buffer pH 7.5, following the protocol used for human MAOs [28]. The assay mixture contained 0.10 mM 4-aminoantipyrine, 1.0 mM 3,5-dichloro-2-hydroxybenzenesulfonate, and 0.013 mg mL^{-1} HRP. Initial assays were carried out to screen different amines as substrates at a final concentration of 4 mM (Table 2). The reaction was started by adding 1.0 µM MAO$_{Tb}$ except for the most active compounds methyl-hexylamine, *n*-hexylamine, and *n*-pentylamine (10 nM MAO$_{Tb}$) and *n*-heptylamine (3 nM MAO$_{Tb}$) to avoid signal overflow. Absorbance changes at 25 °C were monitored at 515 nm (ε_{515} = 26 mM^{-1} cm^{-1}) using a Cary 100 UV–visible spectrophotometer (Agilent, Santa Clara, CA, USA). This assay (in 50 mM HEPES/NaOH pH 7.5) was also used to test the optimal temperature (ranging from 25 to 85 °C) by measuring the k_{obs} with 1.0 mM *n*-heptylamine and 3 nM MAO$_{Tb}$. In the same enzyme/substrate conditions, the optimal pH curve was determined in different buffer conditions (50 mM solutions of sodium citrate, potassium phosphate, TRIS/HCl, HEPES/NaOH, and CHES/NaOH) at pH values ranging from 4 to 10. Moreover, the effect of ionic strength

on enzyme activity was tested with 1.0 mM *n*-heptylamine and 3 nM MAO$_{Tb}$ in 50 mM HEPES/NaOH buffer pH 7.5 by adding different concentrations (10, 50, 100, and 200 mM) of salts (MgCl$_2$, MnCl$_2$, CaCl$_2$, KCl, and NaCl).

Steady-state parameters for MAO$_{Tb}$ were determined with the best substrates by monitoring the oxygen consumption using an Oxygraph plus system (Hansatech Instruments Ltd., Pentney, UK). Measurements were performed in 50 mM potassium phosphate buffer pH 7.5, using between 0.10 and 1.0 µM enzyme, depending on the substrates, while varying the substrate concentration between 0.10 and 150 mM. The reaction chamber had a total volume of 1.0 mL, and the sample was constantly stirred (60 r.p.m.). The reactions were initiated by adding the substrate and subsequently monitored for the initial linear decrease in oxygen concentration. Data collected were analyzed by nonlinear regression curve with GraphPad Prism 8.0 software (La Jolla, CA, USA) using Michaelis–Menten curve model.

Presteady-state kinetics

The rate at which the flavin cofactor of MAO$_{Tb}$ was reduced by substrate was monitored in a nitrogen-purged

anaerobic chamber of a SX20 stopped-flow instrument (Applied Photophysics, Surrey, UK). To assure anoxic conditions, 625 nM glucose and 1.8 mg/mL glucose oxidase were added in the enzyme and substrate solutions, after flushing with nitrogen. The reduction was initiated by mixing 5.0 μM enzyme with *n*-hexylamine solution with substrate concentrations ranging from 50 μM to 25 mM in 50 mM KP_i (pH 7.5) buffer. Upon mixing in the stopped-flow instrument, changes in flavin absorbance were monitored using the photodiode array detector. Reduction in MAO_{Tb} with each substrate concentration was performed in triplicate with spectral scans being collected every millisecond. The obtained data were analyzed using Pro-Kinetics v1.0.13 (Applied Photophysics, Surrey, UK), and the determined reduction rates were subsequently analyzed in GraphPad Prism 6.05 (La Jolla, CA, USA). The reoxidation of MAO_{Tb} was measured using the same equipment where substrate-reduced MAO_{Tb} was first prepared by mixing anaerobically 40 μM MAO_{Tb} with 40 μM *n*-hexylamine. In the stopped-flow instrument, reduced MAO_{Tb} was mixed with aerobic buffer (50 mM KP_i, pH 7.5), resulting in a final oxygen concentration of ∼120 μM. The K_M of oxygen was probed by monitoring the depletion of molecular oxygen in solution under atmospheric pressure (240 μM) by the reaction between an excess of hexylamine (40 mM) with 0.1 μM MAO_{Tb} in KP_i pH 7.5 (25 °C) using an Oxygraph plus system (Hansatech Instruments Ltd., Pentney, UK).

Protein crystallization and structure elucidation

Crystals of MAO_{Tb} were obtained using the sitting drop vapor diffusion technique by mixing equal volumes of protein sample (6.5 mg mL^{-1} in 50 mM potassium phosphate pH 7.5) and a reservoir solution consisting of 22%–30% PEG4000, 100 mM TRIS/HCl buffer pH 8.5, 200 mM $MgCl_2$. Yellow spear-shaped crystals grew in 7–10 days at 20 °C. X-ray diffraction data were collected at the beamtime X06SA (SLS, Villigen, Switzerland). For data collection, crystals were transferred into a mother liquor solution containing 20% (v/v) glycerol and flash-cooled in a stream of gaseous nitrogen at 100 K. Data processing and scaling were carried out using XDS [37] and programs of the CCP4 package [38]. The AlphaFold coordinates of MAO_{Tb} obtained during the genome mining work described above were employed for molecular replacement using MolRep from the CCP4 package [38]. Model building and structure analysis were performed by the program COOT [39], whereas refinement was carried out by REFMAC5 [40]. Tight noncrystallographic symmetry restraints were applied in the first refinement calculation. Data collection and refinement statistics are reported in Table 4. Figures were created by Chimera and ChimeraX [41,42]. Atomic coordinates and structure factors were deposited with the Protein Data Bank (PDB code 8P84).

Author contributions

MWF and CB conceived and supervised the experiment. LB performed steady-state kinetics and elucidated the structure. LLS identified the enzyme with its expression/ purification protocol and carried out the presteady-state kinetics. All authors helped in preparing the manuscript and approve the final version.

Acknowledgments

Conflict of Interest

The authors declare no conflict of interest.

Peer review

The peer review history for this article is available at https://www.webofscience.com/api/gateway/wos/peer-review/10.1111/febs.16973.

Data Availability Statement

Structural data are available in the Protein Data Bank (8P84).

References

1 Santos MHA (1996) Biogenic amines: their importance in foods. *Int J Food Microbiol* **29**, 213–231. doi: 10.1016/0168-1605(95)00032-1

2 Madeo F, Eisenberg T, Pietrocola F & Kroemer G (2018) Spermidine in health and disease. *Science* **359**, doi: 10.1126/science.aan2788

3 Evans P (1980) Biogenic amines in the insect nervous system. *Advances in Insect Physiology* **15**, 317–473. doi: 10.1016/s0065-2806(08)60143-5

4 Brink BT, Damink C, Joosten H & Veld JHI (1990) Occurrence and formation of biologically active amines in foods. *Int J Food Microbiol* **11**, 73–84. doi: 10.1016/0168-1605(90)90040-c

5 Ancín-Azpilicueta C, González-Marco A & Jiménez-Moreno N (2008) Current knowledge about the presence of amines in wine. *Crit Rev Food Sci Nutr* **48**, 257–275. doi: 10.1080/10408390701289441

6 Önal A (2007) A review: current analytical methods for the determination of biogenic amines in foods. *Food Chem* **103**, 1475–1486. doi: 10.1016/j.foodchem.2006.08.028

7 Bóka B, Adányi N, Szamos J, Virág D & Kiss A (2012) Putrescine biosensor based on putrescine oxidase from Kocuria rosea. *Enzyme Microb Technol* **51**, 258–262. doi: 10.1016/j.enzmictec.2012.07.006

8 Ghislieri D, Houghton D, Green AR, Willies SC & Turner NJ (2013) Monoamine oxidase (MAO-N) catalyzed Deracemization of Tetrahydro-β-carbolines: substrate dependent switch in Enantioselectivity. *ACS Catalysis* **3**, 2869–2872. doi: 10.1021/cs400724g

9 Floris G & Agrò AF (2013) Amine Oxidases. In Encyclopedia of biological chemistry, 2nd edn, Academic Press,

10 Fitzpatrick PF (2010) Oxidation of amines by flavoproteins. *Arch Biochem Biophys* **493**, 13–25. doi: 10.1016/j.abb.2009.07.019

11 Dijkman WP, De Gonzalo G, Mattevi A & Fraaije MW (2013) Flavoprotein oxidases: classification and applications. *Appl Microbiol Biotechnol* **97**, 5177–5188. doi: 10.1007/s00253-013-4925-7

12 Tararina MA & Allen KN (2020) Bioinformatic analysis of the Flavin-dependent amine oxidase superfamily: adaptations for substrate specificity and catalytic diversity. *J Mol Biol* **432**, 3269–3288. doi: 10.1016/j.jmb.2020.03.007

13 Shulman KI, Herrmann N & Walker SE (2013) Current place of monoamine oxidase inhibitors in the treatment of depression. *CNS Drugs* **27**, 789–797. doi: 10.1007/s40263-013-0097-3

14 Carpéné C, Boulet N, Chaplin A & Mercader JM (2019) Past, present and future anti-obesity effects of Flavin-containing and/or copper-containing amine oxidase inhibitors. *Medicines* **6**, 9. doi: 10.3390/medicines6010009

15 Wang X, Li B, Kim YS, Wang Y, Li Z, Yu J, Zeng S, Ma X, Choi IH, Di Biase S et al. (2021) Targeting monoamine oxidase a for T cell–based cancer immunotherapy. *Science Immunology* **6**, 59. doi: 10.1126/sciimmunol.abh2383

16 Sturza A, Duicu O, Vaduva A, Danila M, Noveanu L, Varró A & Muntean D (2015) Monoamine oxidases are novel sources of cardiovascular oxidative stress in experimental diabetes. *Can J Physiol Pharmacol* **93**, 555–561. doi: 10.1139/cjpp-2014-0544

17 Schilling B & Lerch K (1995) Amine oxidases from aspergillus Niger: identification of a novel flavin-dependent enzyme. *Biochim Biophys Acta* **1243**, 529–537. doi: 10.1016/0304-4165(94)00183-x

18 Carr R, Alexeeva M, Dawson ME, Gotor-Fernández V, Humphrey CE & Turner NJ (2005) Directed evolution of an amine oxidase for the preparative Deracemisation of cyclic secondary amines. *Chembiochem* **6**, 637–639. doi: 10.1002/cbic.200400329

19 Muellers SN, Tararina MA, Kuzmanovic U, Galagan JE & Allen KN (2023) Structural insights into the substrate range of a bacterial monoamine oxidase. *Biochemistry* **62**, 851–862. doi: 10.1021/acs.biochem.2c005

20 Lasa IR & Berenguer J (1993) Thermophilic enzymes and their biotechnological potential. *Microbiologia* **9**, 77–89.

21 Van Hellemond EW, Van Dijk M, Heuts DPHM, Janssen DB & Fraaije MW (2008) Discovery and characterization of a putrescine oxidase from *Rhodococcus erythropolis* NCIMB 11540. *Appl Microbiol Biotechnol* **78**, 455–463. doi: 10.1007/s00253-007-1310-4

22 Mirdita M, Schütze K, Moriwaki Y, Heo L, Ovchinnikov S & Steinegger M (2022) ColabFold: making protein folding accessible to all. *Nat Methods* **19**, 679–682. doi: 10.1038/s41592-022-01488-1

23 Holm L (2022) Dali server: structural unification of protein families. *Nucleic Acids Res* **50**, W210–W215.

24 Robert X & Gouet P (2014) Deciphering key features in protein structures with the new ENDscript server. *Nucleic Acids Res* **42**, W320–W324. doi: 10.1093/nar/gku316

25 Son S, Ma J, Kondou Y, Yoshimura M, Yamashita E & Tsukihara T (2008) Structure of human monoamine oxidase a at 2.2-Å resolution: the control of opening the entry for substrates/inhibitors. *Proc Natl Acad Sci USA* **105**, 5739–5744. doi: 10.1073/pnas.0710626105

26 Fraaije MW, Pikkemaat M & Van Berkel W (1997) Enigmatic gratuitous induction of the covalent flavoprotein vanillyl-alcohol oxidase in *Penicillium simplicissimum*. *Appl Environ Microbiol* **63**, 435–439. doi: 10.1128/aem.63.2.435-439.1997

27 Gaweska H & Fitzpatrick PF (2011) Structures and mechanism of the monoamine oxidase family. *Biomol Concepts* **2**, 365–377. doi: 10.1515/bmc.2011.030

28 Reis J & Binda C (2023) The peroxidase-coupled assay to measure MAO enzymatic activity. *Methods Mol Biol* **2558**, 23–34. doi: 10.1007/978-1-0716-2643-6_3

29 Binda C, Newton-Vinson P, Hubálek F, Edmondson DE & Mattevi A (2002) Structure of human monoamine oxidase B, a drug target for the treatment of neurological disorders. *Nat Struct Biol* **9**, 22–26. doi: 10.1038/nsb732

30 Voss NR & Gerstein M (2010) 3V: cavity, channel and cleft volume calculator and extractor. *Nucleic Acids Res* **38**, 555–562. doi: 10.1093/nar/gkq395

31 Iacovino LG, Manzella N, Resta J, Vanoni MA, Rotilio L, Pisani L, Edmondson DE, Parini A, Mattevi A, Mialet-Perez J et al. (2020) Rational redesign of monoamine oxidase a into a dehydrogenase to probe ROS in cardiac aging. *ACS Chem Biol* **15**, 1795–1800. doi: 10.1021/acschembio.0c00366

32 Goswami S, Nath P & Datta S (2022) Role of thermophilic cellulases and organisms in the conversion of biomass to biofuels. In Extremozymes and their industrial applications, pp. 85–113. Elsevier eBooks.

33 Jumper J, Evans R, Pritzel A, Green T, Figurnov M, Ronneberger O, Tunyasuvunakool K, Bates R, Žídek A, Potapenko A *et al.* (2021) Highly accurate protein structure prediction with AlphaFold. *Nature* **596**, 583–589. doi: 10.1038/s41586-021-03819-2

34 The PyMOL molecular graphics system, version 2.0 Schrödinger, LLC.

35 Engler C & Marillonnet S (2014) Golden gate cloning. In DNA cloning and assembly methods (Valla S & Lale R, eds), pp. 119–131. Humana Press, doi: 10.1007/978-1-62703-764-8_9

36 Forneris F, Orru R, Bonivento D, Chiarelli LR & Mattevi A (2009) Thermo fad, a Thermofluor®-adapted flavin ad hoc detection system for protein folding and ligand binding. *FEBS Journal* **276**, 2833–2840. doi: 10.1111/j.1742-4658.2009.07006.x

37 Kabsch W (2010) XDS. *Acta Crystallogr D Biol Crystallogr* **66**, 125–132. doi: 10.1107/S0907444909047337

38 Winn MD, Ballard CC, Cowtan KD, Dodson EJ, Emsley P, Evans PR, Keegan RM, Krissinel EB, Leslie AG, McCoy A *et al.* (2011) Overview of the CCP4 suite and current developments. *Acta Crystallogr D Biol Crystallogr* **67**, 235–242. doi: 10.1107/S0907444910045749

39 Emsley P & Cowtan K (2004) Coot: model-building tools for molecular graphics. *Acta Crystallogr D Biol Crystallogr* **60**, 2126–2132. doi: 10.1107/S0907444904019158

40 Murshudov GN, Vagin AA & Dodson EJ (1997) Refinement of macromolecular structures by the maximum-likelihood method. *Acta Crystallogr D Biol Crystallogr* **53**, 240–255. doi: 10.1107/S0907444996012255

41 Pettersen EF, Goddard TD, Huang CC, Couch GS, Greenblatt DM, Meng EC & Ferrin TE (2004) UCSF chimera–a visualization system for exploratory research and analysis. *J Comput Chem* **25**, 1605–1612. doi: 10.1002/jcc.20084

42 Pettersen EF, Goddard TD, Huang CC, Meng EC, Couch GS, Croll TI, Morris JH & Ferrin TE (2021) UCSF ChimeraX: structure visualization for researchers, educators, and developers. *Protein Sci* **30**, 70–82. doi: 10.1002/pro.3943